Electronic Journal of Structural Engineering

Original Article

Cite this: DOI:10.56748/ejse.26929

Received Date: 30 November 2025
Accepted Date: 24 February 2026

1443-9255
https://ejsei.com/ejse

Enhanced Design Approach for Determining Effective Slab Width in Box Girder Composite Sections

Ahmed Adel [a], Mahmoud Lasheen [b*], Amr Shaat [a], Ayman Khalil [a]

[a] Department of Structural Engineering, Ain Shams University, Cairo, Egypt
[b] Concrete Construction Research Institute, Housing and Building National Research Center, Cairo, Egypt
*Corresponding author: mahmoud.lasheen@ahe-consult.com

Abstract

The effective slab width of concrete slabs in Box Girder Composite Sections (BGCSs) has been shown to vary significantly across different loading stages, such as serviceability and ultimate limit states. However, current international design codes do not account for these variations, potentially leading to inaccurate assessments in structural applications. To better understand the behavior of box girders, a nonlinear finite element model of BGCSs was developed using ABAQUS 6.14 (ABAQUS, 2014) and validated against data from three independent experimental research programs. The model successfully predicted the behavior of BGCSs, providing reliable predictions of effective slab width. A comprehensive numerical parametric study was conducted on 216 girders to investigate effective slab widths at the serviceability limit states, considering a range of geometric parameters, including steel girder dimensions and slab thickness. The approach proposed by (Lasheen et al., 2018) for determining the effective slab width in doubly symmetric composite steel sections was adopted and enhanced to be applicable for determining the effective slab width in BGCSs at service limit states. The findings of the second phase demonstrated that the effective slab width is influenced by three factors: the slenderness ratio of the steel box section (L/r_s), the ratio of the slab thickness to the slab width (t_s/B_s), and the ratio of the slab width to the girder span (B_s/L). Consequently, a newly developed design equation is proposed in the current research to accurately calculate the effective slab widths at service limit states.

Keywords

Steel-concrete composite bridge, Box girder, Numerical analysis, Effective slab width, Bridges

1. Introduction

The concrete slab in a steel–concrete composite box girder is typically subjected to non-uniform longitudinal stresses across its width, as shown in Fig. 1. This non-uniformity results primarily from the shear flow transferred between the concrete slab and the steel section. This phenomenon, known as shear lag (Chen et al., 2019), (Zhu et al., 2015), (Nicoletti et al., 2021), (Sedlacek & Bild, 1993) & (Gara et al., 2001), significantly affects the stress distribution and, consequently, the effective slab width. If not properly accounted for, shear lag may lead to unconservative stress estimation, excessive deflections, and inefficient material utilization in wide-deck bridge systems.

Early analytical and experimental studies on composite beams established the fundamental concept of effective width and its dependence on shear lag behavior. (A. O. Adekola, 1968) provided one of the earliest experimental and analytical formulations for evaluating the effective width of steel–concrete composite beams, clearly demonstrating the non-uniform stress distribution across the slab. This was followed by (A. O. Adekola, 1974), who investigated the influence of partial interaction and shear connector behavior on shear lag development, highlighting the coupled role of interface slip and longitudinal stress redistribution. These pioneering works laid the foundation for subsequent analytical models adopted in early composite beam design practice.

Subsequent research further clarified the role of deck stiffness, loading conditions, and boundary effects in governing shear lag behavior. (Gara et al., 2008) extended shear lag investigations to composite bridge systems with complex static schemes by employing deck-based finite element models, providing improved insight into stress redistribution mechanisms under realistic loading conditions. Their study demonstrated that simplified beam-based approaches may significantly underestimate shear lag effects in wide composite decks. More recently, (Huitong et al., 2019) proposed a simplified analytical method that explicitly accounts for shear lag effects in steel–concrete composite decks, offering a computationally efficient alternative for preliminary design and assessment.

Recent numerical and analytical advancements by (G.F. Giaccu et al., 2022) & (G.F. Giaccu et al., 2025) further contributed to the understanding of effective slab width and shear lag effects in composite beams and cable-stayed bridges subjected to combined bending and compression. Their work emphasized the limitations of conventional effective width expressions when applied to complex bridge geometries and serviceability limit states. Despite these advances, most existing formulations and simplified approaches have been developed primarily for composite I-girder systems or symmetric cross-sections and may not be directly applicable to composite box girders with wide decks and large web spacing.

According to the American Association of State Highway and Transportation Officials (AASHTO, 2017), Clause 6.10.1.1.1e limits the effective slab width of steel–concrete interior composite I-girders to the smallest of the following values: one-quarter of the girder span, the center-to-center spacing of adjacent girders, or twelve times the slab thickness. These provisions are largely empirical and implicitly assume relatively narrow decks and closely spaced girders, conditions that are often unlike the parameters governing the behavior of modern long-span composite box girder bridges. However, the AASHTO (2017) provisions provide no specific guidance for determining the effective slab width of composite box girders.

In contrast, the European Standard (Eurocode 4, 2005) requires the effective slab width to be determined using the provisions of Clause 5.4.1.2, whereby for sections at mid-span or at internal supports, the effective width may be calculated using Eq. (1).

$$b_{eff} = b_0 + \sum b_{ei} \quad (1)$$

Where b_0 is the distance between headed shear studs, and b_{ei} represents the effective slab width measured from each side of the beam center. Although (Eurocode 4, 2005) introduces a more mechanics-based framework rooted in shear lag theory originally developed for composite beams, it does not explicitly account for the unique stress redistribution mechanisms, wide deck behavior, and asymmetric geometry inherent in composite box girder systems. The shear lag effect reduces the structural efficiency of BGCSs by increasing stress concentrations near the intersection of the web centerline and the flange, which results in lower axial stresses at the mid-width of the cross-section. Consequently, this may lead to increased lateral deflection, as illustrated in Fig. 1.

The severity of shear lag increases as the distance between the webs becomes larger, a condition commonly encountered in modern wide single-cell box girders. The effect also becomes more pronounced when the ratio of box width to span length increases (Alemayehu, 2013). In addition, shear lag develops in the steel bottom flange due to warping displacements induced by longitudinal bending, particularly in sections subjected to large, concentrated loads or those incorporating wide and thin bottom flanges (Yao & Chung, 2002).

The effective slab width is typically obtained by integrating the non-uniform longitudinal stresses along the slab width and steel bottom flange. Nevertheless, international design codes provide no explicit provisions for

estimating the effective slab width of composite box girders, offering guidance only for composite I-girders. This gap has motivated several experimental and numerical investigations.

For example, (Kamar et al., 2021) examined the influence of slip and stress distribution in composite beams, demonstrating the distinct stress patterns at the steel–concrete interface compared with concrete–concrete interfaces (Fig. 2). Similarly, (Lasheen et al., 2016) highlighted the strong dependence of the effective slab-width-to-span ratio on the steel beam slenderness ratio (L/r_s) and proposed design equations for estimating both effective width and interface slip. Other studies further confirmed that the stiffness of the steel section, particularly the behavior of the bottom flange, which is fully effective in tension plays a significant role in defining the effective slab width (Lasheen et al., 2018).

To improve the design of BGCSs, numerical investigations have been conducted to study their behavior under bending as a function of geometry and span. These studies are essential for optimizing design practices, as BGCSs remain widely used due to their structural efficiency, long-span capability, and favorable economic performance. Despite the challenges associated with shear lag and the absence of specific code provisions, accurately determining the effective slab width is crucial for achieving reliable and optimized BGCS designs.

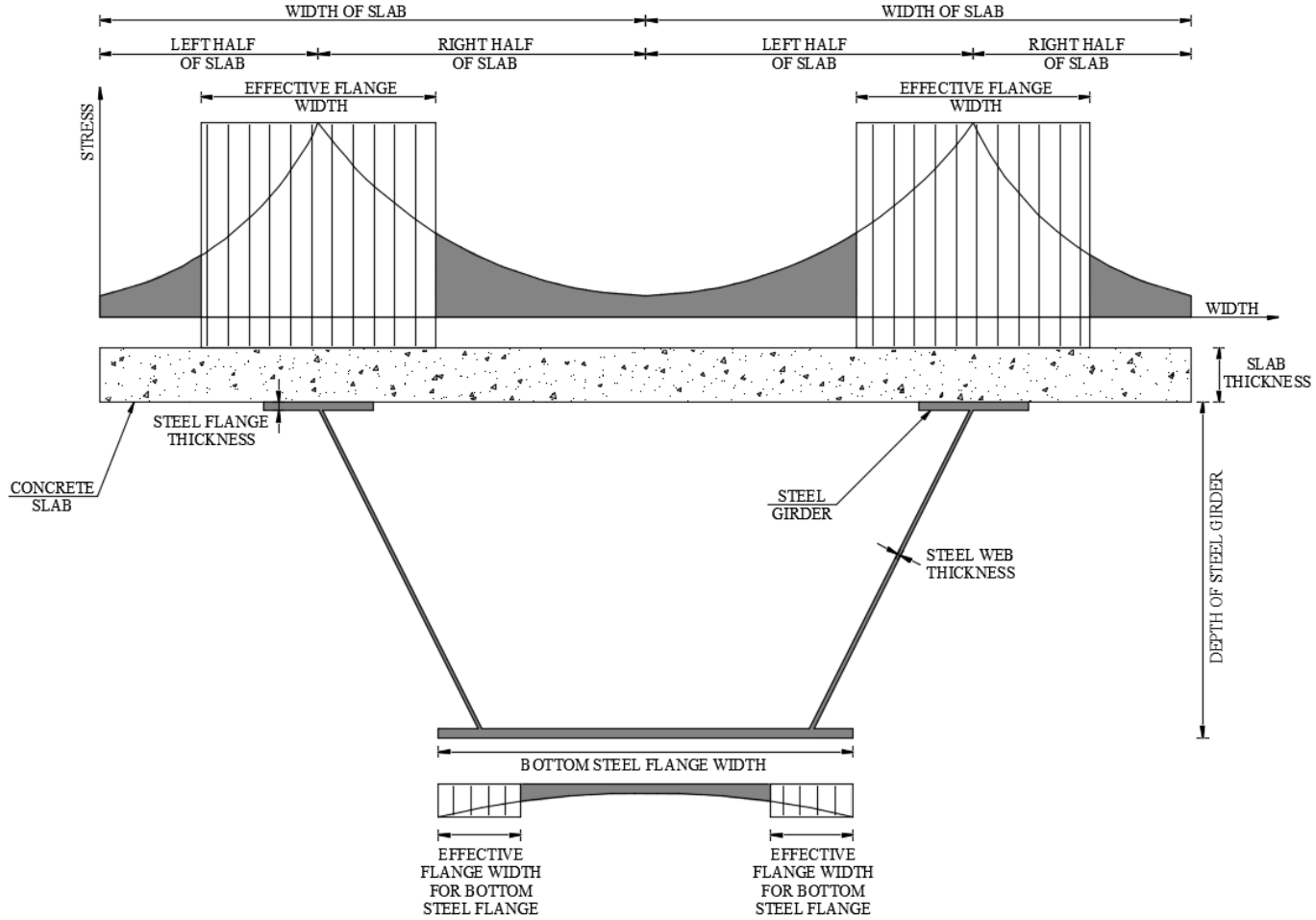

Fig. 1 BGCS longitudinal stresses.

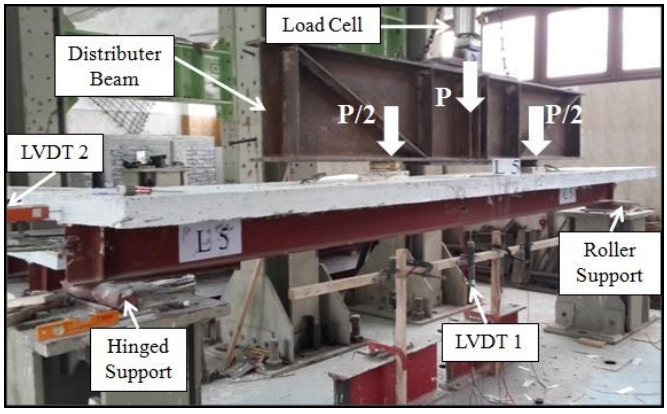

(a) Lasheen et al. (2016)

(b) Ryu et al. (2004)

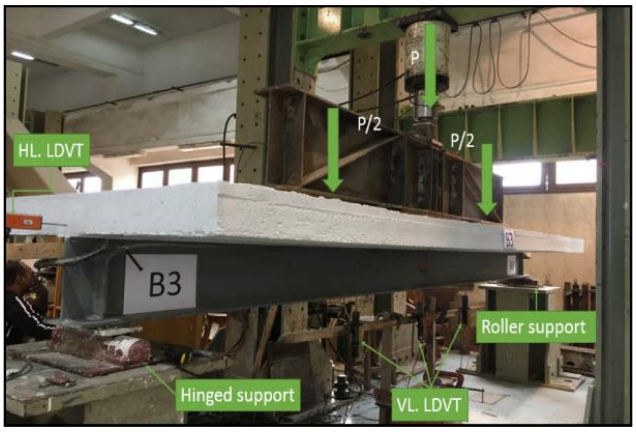

(c) kamar et al. (2021)

Fig. 2 Experiment programs used for the FEM verification.

2. Finite element model

A non-linear finite element model was developed to simulate the structural behavior of steel–concrete composite box girders. The model was created using Abaqus 6.14 (ABAQUS, 2014), and a comprehensive parametric study was conducted on 216 simply supported BGCS specimens. Due to symmetry in geometry, loading, and boundary conditions, only one-half of each girder was modeled; quarter-symmetry could not be adopted because BGCSs are not monosymmetric, as illustrated in Fig. 4.

The dimensions of the steel box girder were established in accordance with the (AASHTO, 2017) specifications. The concrete slab, steel box girder, and shear connectors were modeled using C3D8R solid elements, each comprising eight nodes with three translational degrees of freedom per node. Reinforcement bars were represented using T3D2 truss elements with two nodes and three degrees of freedom per node. A maximum global mesh size of 200 mm was used for all finite element models.

2.1 Material model

Concrete modeling

The concrete used in this study has a compressive strength of 27 MPa and a Young's modulus of 28 GPa. The Concrete Damage Plasticity (CDP) model was adopted, with tension stiffening incorporated to represent the post-cracking tensile behavior and to capture the strain-softening response of cracked concrete. Previous studies commonly assumed the total tensile strain at zero stress to be ten times the cracking strain; however, this approach has been shown to be unsuitable for concrete slabs in composite sections (Baskar et al., 2002) & (Liang et al., 2004). (Liang et al., 2005) recommended using a total tensile strain of 0.1 for reinforced concrete slabs in BGCSs. This value reflects the combined effects of distributed cracking, reinforcement restraint, and composite action, and has been shown to provide stable numerical convergence while realistically capturing tension stiffening behavior under serviceability limit state conditions to ensure a realistic representation of post-cracking behavior without early loss of slab stiffness, as illustrated in Fig. 3.

Steel modeling

A bi-linear stress–strain model was adopted for all steel components, including the steel box girder, shear connectors, and reinforcing bars. The elastic properties assigned to the steel were a Young's modulus of 205 GPa and a Poisson's ratio of 0.3. The material was characterized by a yield strength of 300 MPa and an ultimate strength of 520 MPa.

2.2 Steel-concrete interaction

The interaction between the constituent elements was modeled in Abaqus 6.14 (ABAQUS, 2014) using the interaction and surface-to-surface contact techniques. The bond between the concrete slab and the internal steel reinforcement was represented using the truss-in-solid approach, in which the concrete slab acts as the host region modeled with solid elements, while the reinforcement bars are embedded as truss elements.

Surface-to-surface contact was employed to model the interfaces between the concrete slab and the channel shear connectors, as well as between the underside of the slab and the top flange of the steel box girder. The channel connectors were defined as the master surface and the concrete slab as the slave surface. Similarly, the upper steel flanges were assigned as the master surface with the concrete slab again acting as the slave surface.

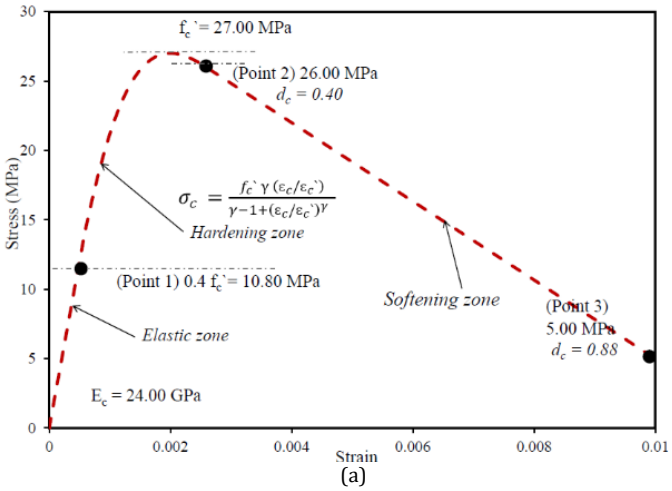

(a)

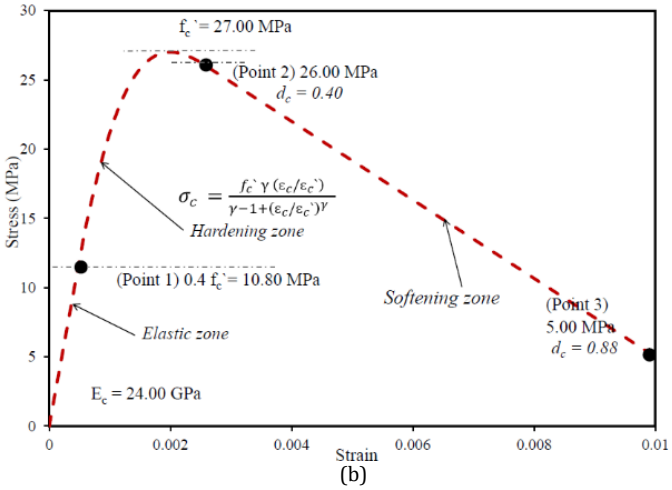

(b)

Fig. 3 Compressive stress-strain (a) and tensile stress-strain curves (b) of concrete.

Normal contact behavior was defined using a hard contact pressure–overclosure relationship, which prevents interpenetration while allowing separation when tensile stresses develop. This formulation enables the model to realistically capture potential uplift or separation at the steel–concrete interface under bending. Tangential behavior was modeled using a penalty friction formulation with a friction coefficient of 0.5, a value widely adopted in the literature to represent frictional resistance at steel–concrete interfaces under serviceability-level loading conditions. This modeling approach permits limited interfacial slip prior to the full mobilization of shear connector resistance, therefore, representing partial interaction behavior rather than assuming idealized full composite action. Welded regions, such as the welds between the shear connectors and the steel flanges and those between the stiffeners and the girder webs, were modeled using tie constraints to ensure full compatibility and to prevent separation at the weld locations.

2.3 Boundary condition

In the current analysis, all girders were modeled as simply supported. Accordingly, vertical and lateral displacements at the supports were restrained. A rigid support was modeled using solid elements. The support block, measuring 250 mm in length and 250 mm in height, was placed beneath the end bearing stiffener. This block was restrained against translation and rotation in the y-direction, as well as rotation in the z-direction, in order to simulate a hinged support and to reduce stress concentration in the thin lower flange of the steel box girder. The boundary conditions of the modeled girders are shown in Fig. 4.

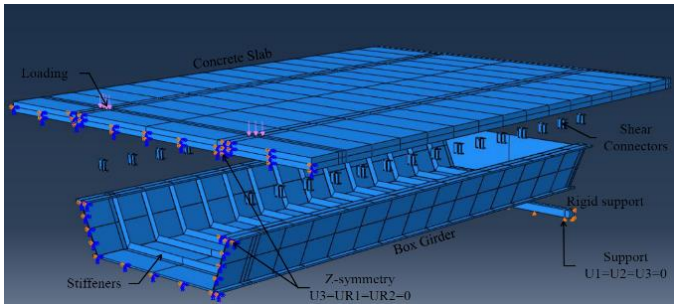

Fig. 4 Finite element mesh of half of BGCS.

3. Validation of the finite element model

The developed finite element model was validated against eight beams tested by (Lasheen et al., 2016), one composite girder tested by (Ryu et al., 2004), and ten beams tested by (Kamar et al., 2021), as shown in Fig. 2. The specimens tested by (Lasheen et al., 2016) consisted of simply supported steel–concrete composite I-section beams with spans of 4800 mm, 2800 mm, and 1800 mm. Ryu et al. (2004) examined a steel–concrete composite box girder bridge composed of two continuous spans of 10,000 mm each. The specimens tested by (Kamar et al., 2021) were simply supported steel–concrete composite I-section beams with a span of 4800 mm.

Lasheen et al. (2016) investigated the effect of the steel section slenderness ratio on the effective slab width in the positive moment region and proposed a design equation applicable to both ultimate and service limit states. Ryu et al. (2004) studied the stress distribution in the negative moment zone and presented design methodologies for cracked and uncracked sections at ultimate and service limit states. Kamar et al. (2021) demonstrated that composite beams with channel shear connectors exhibit higher ultimate load capacity than those with angle connectors, and that the presence of upper steel reinforcement helps prevent longitudinal cracking and promotes full plastification of the steel section.

For validation, numerical and experimental results were compared at critical locations where the maximum responses were expected. As illustrated in Figs. 5 to 7, the numerical predictions show very good agreement with the experimental data. Therefore, the finite element model can be considered reliable for use in the subsequent parametric study.

4. Parametric study

This section presents the parametric study conducted to investigate the key parameters influencing the behavior and design of BGCSs. A total of 216 girders were analyzed. The primary variables considered were the span length, girder depth, slab thickness (t_s), and the top distance between the girder webs (B_{top}). The selected ranges of these parameters were deliberately chosen to reflect typical design practices in steel–concrete composite box girder bridges and to ensure that the study results are directly applicable to real-world engineering applications.

The investigated spans were 10 m, 15 m, 20 m, 24 m, 30 m, and 40 m, while the girder depths examined were 1000 mm, 1500 mm, and 2000 mm. This span range captures varying levels of girder slenderness, with span-to-depth ratios ranging from 1/5 to 1/40, which are critical for evaluating serviceability behavior and shear-lag effects for different applications of BGCSs in structural engineering.

The top distances between webs (B_{top}) considered in the study were 6000 mm, 6500 mm, and 7000 mm. Slab thicknesses of 250 mm, 300 mm, 350 mm, and 400 mm were also examined; this range corresponds to slab span-to-thickness ratios from 1/15 to 1/28.

The ratio between B_{top} and Bb_{ot} was selected to satisfy the (AASHTO, 2017) requirement that the inclination of the web plates relative to a plane normal to the bottom flange must not exceed 1:4. Accordingly, the bottom distances between webs (Bb_{ot}) were taken as 4800 mm, 5200 mm, and 5600 mm. All the variables considered in this study are summarized in Table 1.

All girders were modeled as simply supported. Channel sections (UPN 200) were used as shear connectors to provide full composite action between the concrete slab and the steel box girder. The channel connector length was fixed at 300 mm for all configurations, as illustrated in Fig. 8. All specimens were subjected to four-point bending.

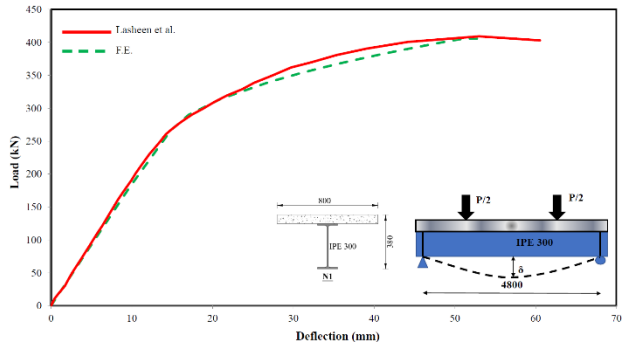

(a)

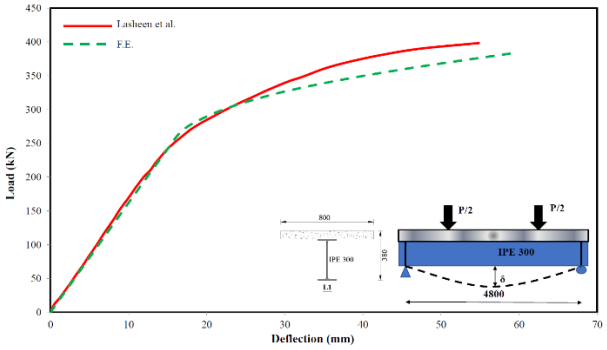

(b)

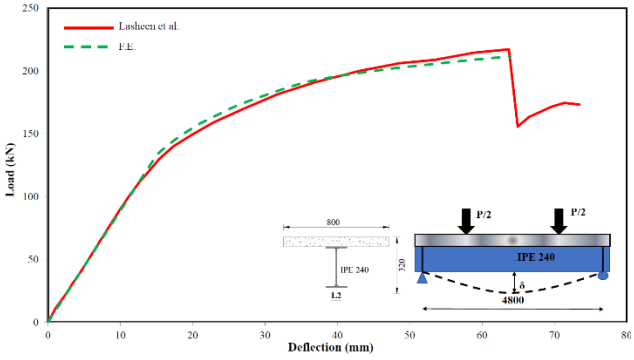

(c)

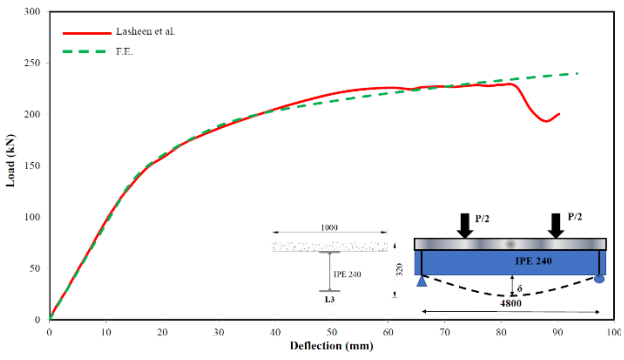

(d)

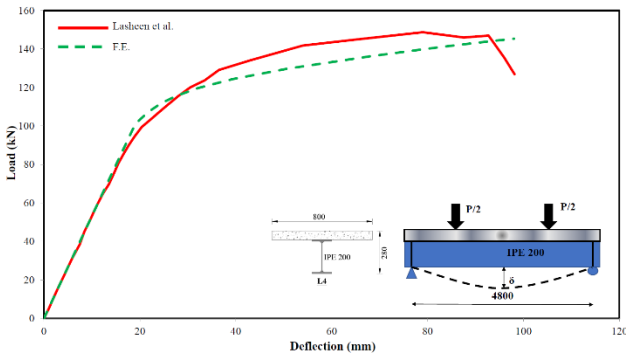

(e)

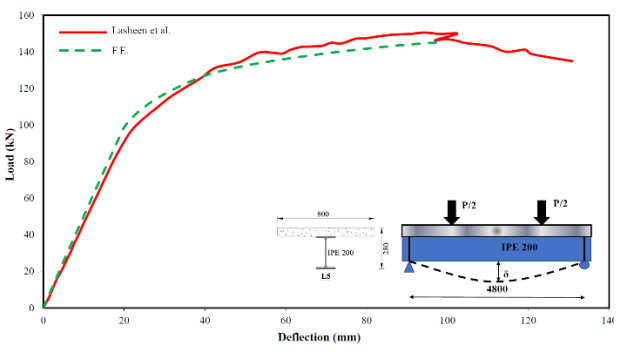

(f)

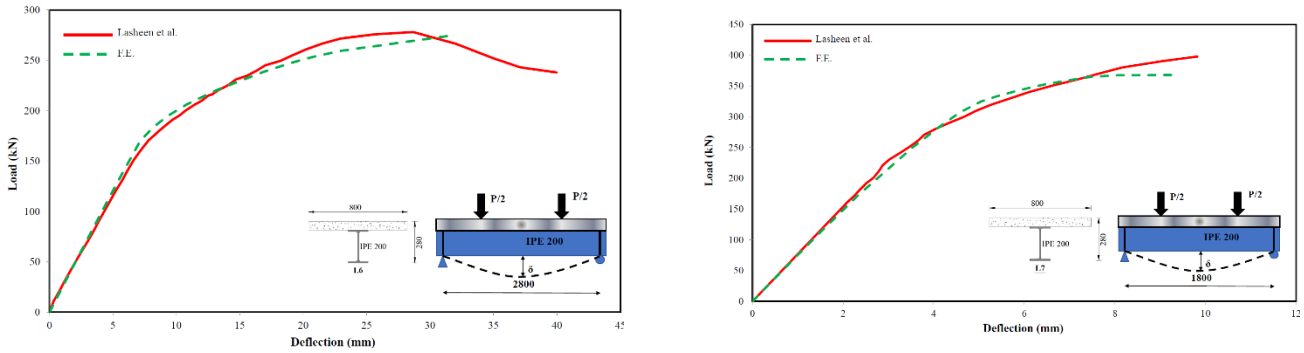

(g) (h)

Fig. 5 FEM versus Exp. result by Lasheen et al (2016)

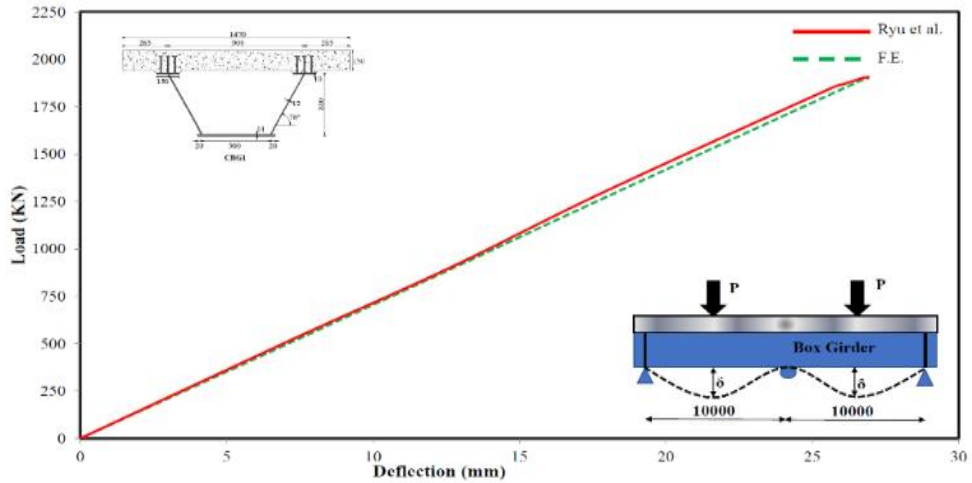

Fig. 6 FEM versus Exp. result by Ryu et al (2004)

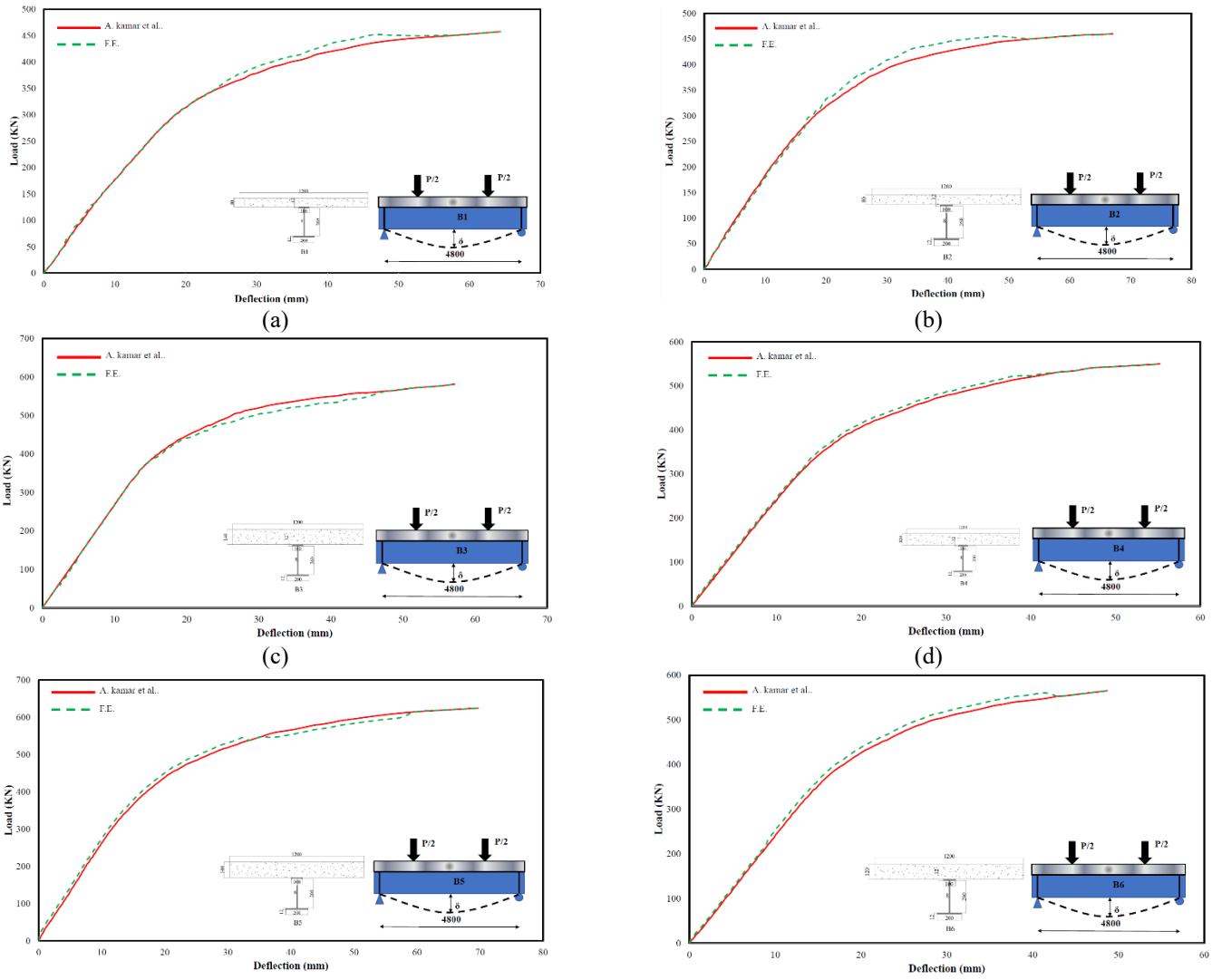

(a) (b)

(c) (d)

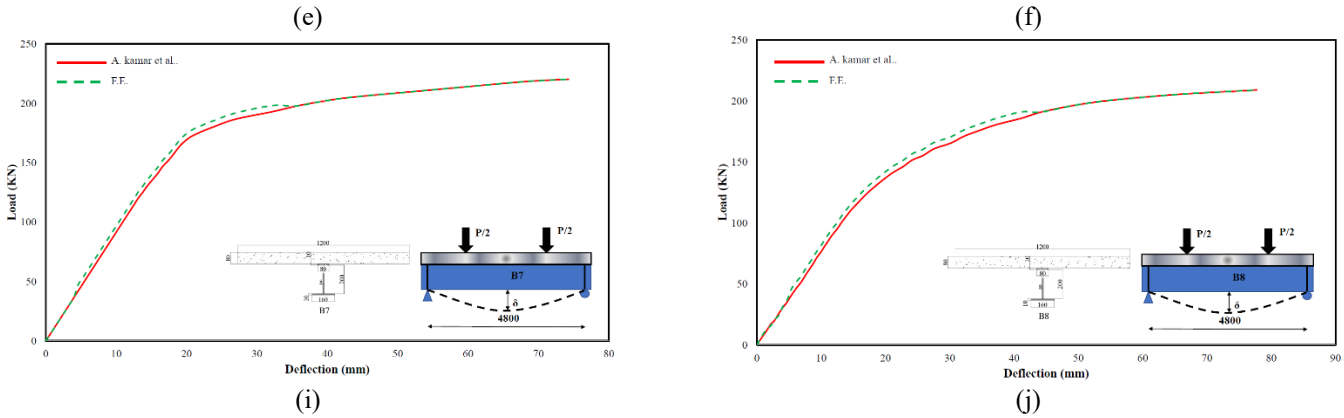

Fig. 7 FEM versus Exp. result by kamar et al. (2021)

Table 1 Details of girders in parametric study

Btop (mm)		6000						6500							7000					
Span (m)		10	15	20	24	30	40	10	15	20	24	30	40		10	15	20	24	30	40
Depth (mm)	Slab thick. (mm)																			
1000	250	B1	B2	B3	B4	B5	B6	B7	B8	B9	B10	B11	B12	B13	B14	B15	B16	B17	B18	
	300	B19	B20	B21	B22	B23	B24	B25	B26	B27	B28	B29	B30	B31	B32	B33	B34	B35	B36	
	350	B37	B38	B39	B40	B41	B42	B43	B44	B45	B46	B47	B48	B49	B50	B51	B52	B53	B54	
	400	B55	B56	B57	B58	B59	B60	B61	B62	B63	B64	B65	B66	B67	B68	B69	B70	B71	B72	
1500	250	B73	B74	B75	B76	B77	B78	B79	B80	B81	B82	B83	B84	B85	B86	B87	B88	B89	B90	
	300	B91	B92	B93	B94	B95	B96	B97	B98	B99	B100	B101	B102	B103	B104	B105	B106	B107	B108	
	350	B109	B110	B111	B112	B113	B114	B115	B116	B117	B118	B119	B120	B121	B122	B123	B124	B125	B126	
	400	B127	B128	B129	B130	B131	B132	B133	B134	B135	B136	B137	B138	B139	B140	B141	B142	B143	B144	
2000	250	B145	B146	B147	B148	B149	B150	B151	B152	B153	B154	B155	B156	B157	B158	B159	B160	B161	B162	
	300	B163	B164	B165	B166	B167	B168	B169	B170	B171	B172	B173	B174	B175	B176	B177	B178	B179	B180	
	350	B181	B182	B183	B184	B185	B186	B187	B188	B189	B190	B191	B192	B193	B194	B195	B196	B197	B198	
	400	B199	B200	B201	B202	B203	B204	B205	B206	B207	B208	B209	B210	B211	B212	B213	B214	B215	B216	

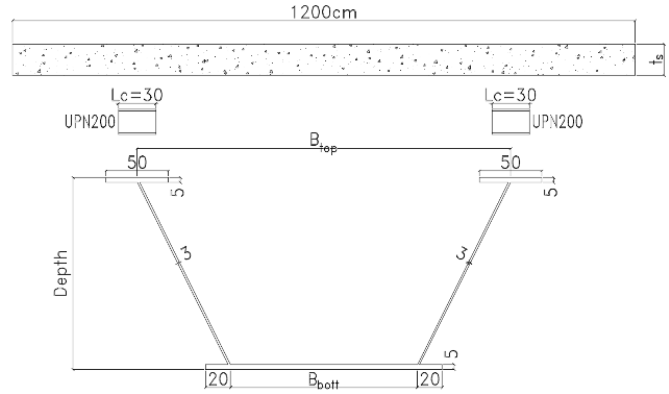

Fig. 8 Box girder configuration dimensions in (cm)

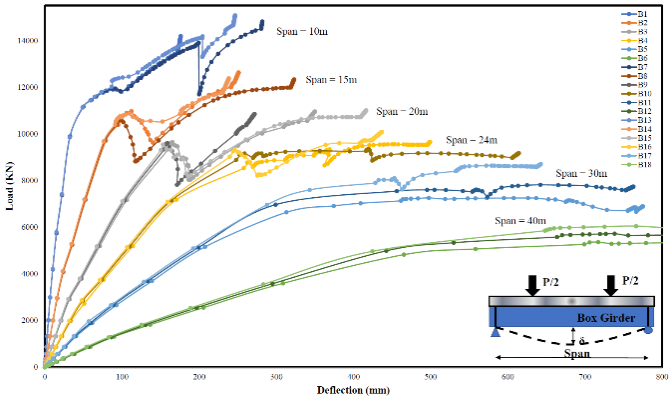

Fig. 9 Load versus mid-span deflection for girders B1 to B18

5. Finite Element model Results

This section presents the results of all BGCS finite element models examined in the study. The outcomes are expressed in terms of load–stress, load–strain, and load–deflection responses, and are compared with the code provisions of (AASHTO, 2017). Figures 9 to 11 show representative results for girders B1 to B18. The ultimate loads for all girders are listed in Table 1A in Annexure, while the effective slab widths calculated at the service limit state using Eq. (9) are provided in Table 2A in Annexure.

Figures 9 to 11 present the load–deflection curves, the strain in the lower steel flange, and the strain in the top concrete surface, respectively. The results show that short-span girders (B1, B2, B3, B7, B8, B9, B13, B14, and B15) exhibit a sudden drop in load capacity at approximately 90 percent of the peak load, occurring immediately after failure. In contrast, long-span girders (B4, B5, B6, B10, B11, B12, B16, B17, and B18) display a smoother post-peak response with gradual reduction in load.

This difference in behavior is attributed to the higher brittleness of short-span girders. In short spans, concrete crushing occurs before yielding of the lower steel flange, resulting in sudden failure. For long spans, yielding of the lower flange precedes concrete crushing, producing a more ductile response. The underlying cause is the shear lag effect, which is more significant in shorter spans. Consequently, short spans have a smaller effective slab width, leading to higher stress concentrations and sudden concrete crushing.

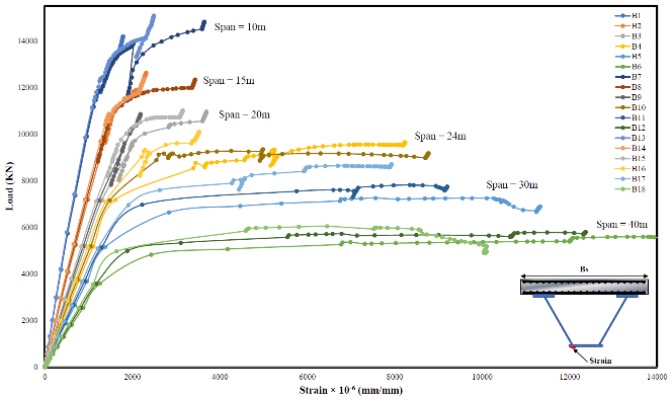

Fig. 10 Load versus lower steel flange strain for girders B1 to B18

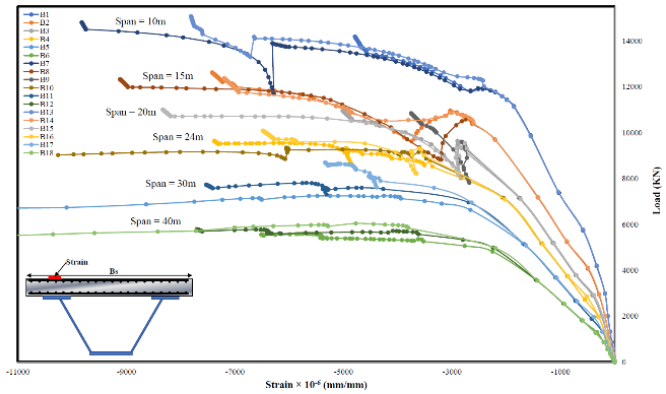

Fig. 11 Load versus top concrete strain for girders B1 to B18

5.1 Effect of steel-concrete box girders inertia on the effective slab width

To examine the influence of steel girder inertia on the effective slab width, several girder section sizes were analyzed. The results, presented in Fig. 12, show that the effective slab width at the service limit state increases as the major-axis moment of inertia of the steel girder increases, for a given concrete slab width. For each girder depth (100 cm, 150 cm, and 200 cm), an increase in the steel girder moment of inertia results in a noticeable increase in the average effective slab width. This demonstrates the important role of steel girder stiffness in determining the effective slab width. Accordingly, it is necessary to establish a clear relationship between the girder inertia and the corresponding effective slab width.

5.2 Effect of steel-concrete box girders' slenderness ratio on the effective slab width

To investigate the relationship between the effective slab width at the service limit state and the steel girder slenderness ratio, the steel girder size and available slab width were evaluated in conjunction with the girder span. The slenderness ratio is expressed as L/r_s, where r_s is the radius of gyration of the steel section about the x–x axis and serves as an indicator of girder size. The effective slab width is expressed in non-dimensional form as B_e/L.

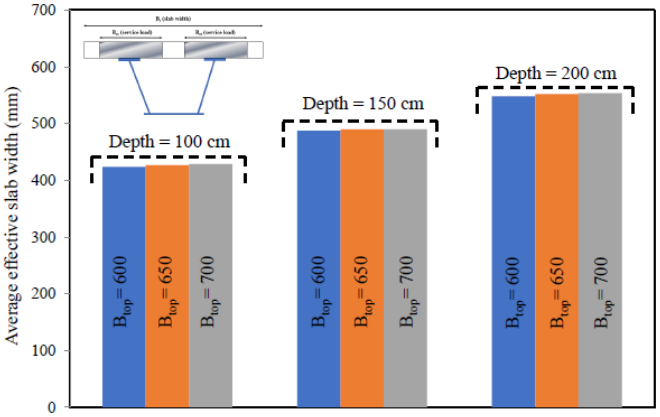

Fig. 12 Effective slab width with various girders.

Figure 13 illustrates the correlation between the slenderness ratio and the effective slab-width-to-span ratio at the service limit state, for six different slab-width-to-span ratios ranging from 0.15 to 0.60. The relationship is presented at service load levels only, as this loading stage exhibits the most significant sensitivity to shear lag.

The results show a clear inverse relationship: as the girder slenderness ratio increases, the effective slab-width-to-span ratio decreases for all slab-width-to-span values. This indicates that more slender girders are less effective in achieving the full slab width under service conditions. Power-function trendlines were used to fit the calculated data, and the resulting curves exhibit excellent agreement, with coefficients of determination (R^2) ranging from 0.95 to 0.99. This reflects a strong correlation between the proposed functional relationship and the computed values.

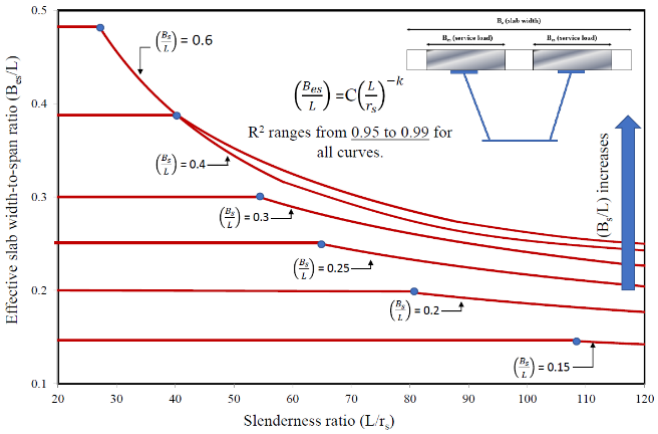

Fig. 13 Effect of steel girder slenderness ratio on the effective slab width.

5.3 Effect of slab thickness on the effective slab width

Four different slab thicknesses were examined to evaluate their influence on the effective slab width. As shown in Fig. 15, the effective slab width at the service limit state increases as the slab thickness decreases, for the same available concrete slab width. The thinner slabs exhibit larger effective widths, indicating a more uniform longitudinal stress distribution across the slab width. This demonstrates that slab thickness plays a significant role in determining the effective slab width. The trend is attributed to the calculation of the total compressive force in the slab (Cslab), which is obtained using Eq. (2).

$$C_{Slab} = \sum_{i=1}^{n} \sigma_i . A_i \tag{2}$$

where "n" is the number of slab elements, "i" is the element number, "σ_i" is the longitudinal stress at each element, and

"A_i" is the cross-sectional area of the element "i", as shown in Fig. 14. The effective flange width can be computed using equation (3).

$$B_{es} = \frac{C_{slab}}{max\ stress \times slab\ thickness} = \frac{C_{slab}}{\frac{\sum \sigma_i}{n} \times t} \tag{3}$$

where B_{es} is the total effective slab width for one girder, and t is the total slab thickness. Therefore, establishing a relationship between the slab thickness and the effective slab width is necessary.

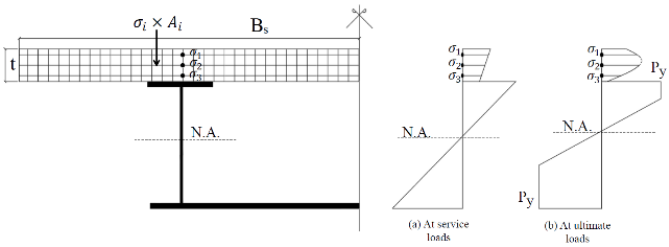

Fig. 14 Stress distribution along slab thickness.

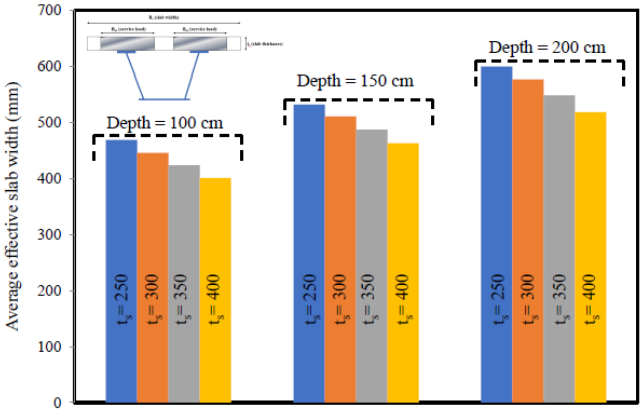

Fig. 15 Effective slab width with various girders.

5.4 Effect of shear lag in steel bottom flange on the effective slab width

Four different values of the top distance between the girder webs were analyzed to investigate the influence of shear lag in the steel bottom flange on the effective slab width. The ratio of the moment of inertia about

the y–y axis to that about the x–x axis was used as an indicator of shear lag sensitivity, as illustrated in Fig. 16. The results show that even when this inertia ratio reaches its maximum, the effect of shear lag in the steel bottom flange on the effective slab width remains negligible.

This minimal influence aligns with established design code provisions, which traditionally disregard the contribution of the steel bottom flange when calculating the effective slab width in composite girders. As a result, the effective slab width for steel–concrete composite box girders remains comparable to that of composite I-section girders, since the bottom flange does not significantly alter the load distribution or the effective width.

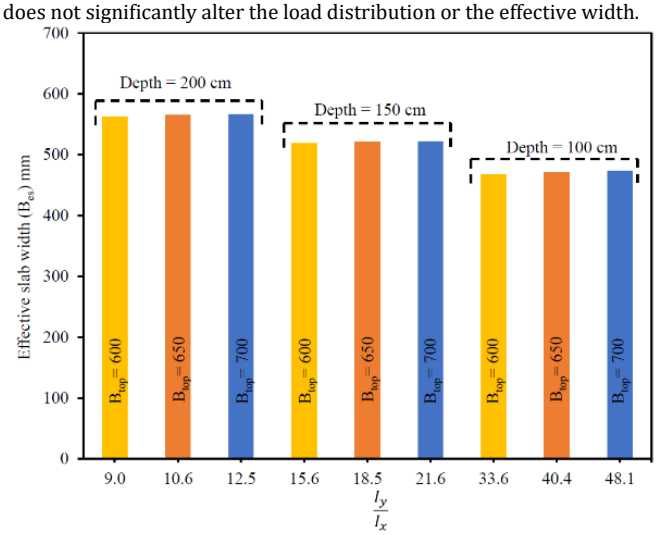

Fig. 16 Effective slab width versus l_y/l_x

6. Design guidelines

This section presents design guidelines for determining the effective slab width of steel box girders at the service limit state. The methodology proposed by (Lasheen et al., 2018) for doubly symmetric composite steel sections was adopted and extended to make it applicable to BGCSs. Lasheen et al. (2018) introduced two equations for calculating the effective slab width at both the service and ultimate limit states. However, in the present study, design recommendations are provided only for the service limit state, since the entire slab width becomes fully effective at the ultimate limit state.

The modified design equation proposed in this study was developed based on a best-fit analysis of the finite element results. These results were validated against three independent experimental programs conducted by (Macorini et al., 2006), (Lasheen et al., 2016) and (Kamar et al., 2021). To assess the performance of the proposed equation, its predictions of the effective slab width at the service limit state (B_{es}) were compared with the values obtained using the provisions of (AASHTO, 2017) and (Eurocode 4, 2005).

6.1 Proposed design equation for effective slab width at service limit states (B_{es})

The design guidelines developed by (Lasheen et al., 2018) were adopted as the foundation for the current study and are expressed in Eq. (4):

$$\left(\frac{B_{es}}{L}\right) = M\left(\frac{B_s}{L}\right)\left(\frac{L}{r_s}\right)^{-k} \leq \frac{B_s}{L} \tag{4}$$

Equation (4) introduces two parameters, M and K, where M was assumed to be a constant equal to 2.5 in Lasheen et al. (2018), as expressed in Eq. (5). In contrast, factor K is a dimensionless coefficient that quantifies the sensitivity of the effective slab width to girder slenderness through the slab width-to-span ratio. Specifically, when the available slab width is relatively small, the influence of girder slenderness on the effective slab width becomes limited; conversely, as the slab width increases, the effect of girder slenderness becomes more pronounced.

It is evident from Eq. (4) that (Lasheen et al., 2018) did not account for the influence of slab thickness. This omission is associated with the limited span lengths examined in their study, which did not exceed 7.2 m. As a result, the effective slab width in their work was primarily governed by the span rather than by the thickness of the concrete slab.

In contrast, the present study demonstrates that slab thickness has a noticeable influence on the effective slab width at the service limit state, particularly because the girder spans, considered in this study, range from 10 m to 40 m. Therefore, a range of slab thicknesses was incorporated into the analysis.

Despite the fact that the value of "M" was taken as constant in the study by Lasheen et al. (2018) due to the absence of slab thickness as a governing parameter, in the current study the value of M varies with slab thickness and ranges approximately from 2.94 to 3.36 across all slab-width-to-span ratios, as summarized in Table 2. Figure 17 illustrates the variation of factor M, clearly indicating that it cannot be assumed constant for BGCSs.

$$\left(\frac{B_{es}}{L}\right) = 2.5\left(\frac{B_s}{L}\right)\left(\frac{L}{r_s}\right)^{-K} \leq \frac{B_s}{L} \tag{5}$$

The factor "M" for each slab-width-to-span ratio was replaced by the expression "Q $(t_s/B_s)^{-Y}$" to account for different slab thicknesses, whereby the physical meaning of the factor "M" is considered to represent the effect of slab thickness on the effective slab width value. The factors Q and Y are dimensionless factors and are used to examine the sensitivity of other parameters (i.e., B_s/L or L/r_s) to the level of the effect of slab thickness to slab width on the effective slab width value.

Consequently, the factor "K" must be recalculated based on this modified formulation of the factor "M". To express the equation in its final form, two new parameters, "Q" and "Y", are introduced. These parameters depend on the ratio of slab thickness to slab width (t_s/B_s), as presented in Table 3.

Table 3 shows that the factor "M" increases as the ratio "Q $(t_s/B_s)^{-Y}$" decreases. This trend indicates that the effect of slab thickness on the effective slab width becomes significant when different slab thicknesses are considered. Therefore, the final form of the proposed equation is expressed in Eq. (6).

$$\left(\frac{B_{es}}{L}\right) = Q\left(\frac{t_s}{B_s}\right)^{-Y}\left(\frac{B_s}{L}\right)\left(\frac{L}{r_s}\right)^{-k} \leq \frac{B_s}{L} \tag{6}$$

For simplicity, a non-linear expression for the factor "M" was developed in terms of the slab-thickness-to-slab-width ratio, as presented in Eq. (7). The curve, shown in Fig. 18, was fitted using an exponential function and achieved an R^2 value of 0.99.

$$M = 1.33\left(\frac{t_s}{B_s}\right)^{-0.29} \tag{7}$$

Table 2 highlights the values of the factor "K" and the slab-width-to-span ratio. It is clear that the factor "K" increases as the slab-width-to-span ratio increases, which is consistent with the findings of (Lasheen et al., 2018), as expressed in Eq. (8). The same factor was examined and adopted in the present study. As shown in Fig. 19, the fitted curve produced an R^2 value of 0.99, indicating an excellent correlation.

$$K = 0.358\left(\frac{B_s}{L}\right)^2 + 0.145\left(\frac{B_s}{L}\right) + 0.233 \tag{8}$$

Therefore, the final form of the equation can be expressed in Eq. (9)

$$\left(\frac{B_{es}}{L}\right) = 1.33\left(\frac{t_s}{B_s}\right)^{-0.29}\left(\frac{B_s}{L}\right)\left(\frac{L}{r_s}\right)^{-k} \leq \frac{B_s}{L} \tag{9}$$

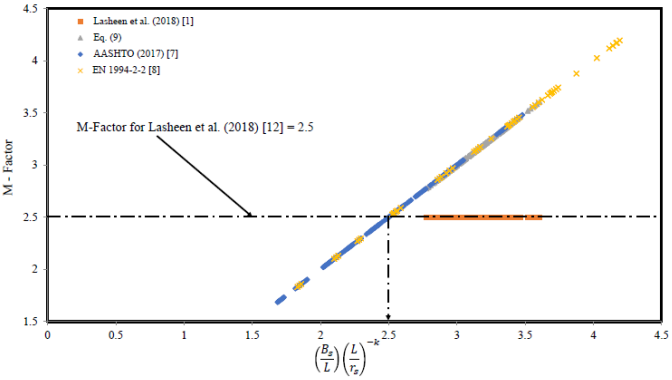

Fig. 17 M Factor for FEA versus code provision & researches for effective slab width at service limits states (B_{es}).

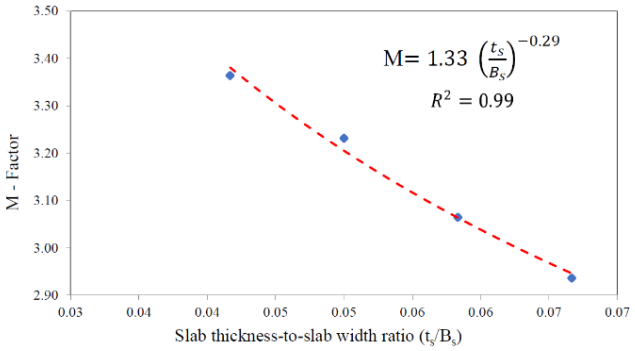

Fig. 18 The factor "M" against the slab thickness -to slab width (t_s/B_s)

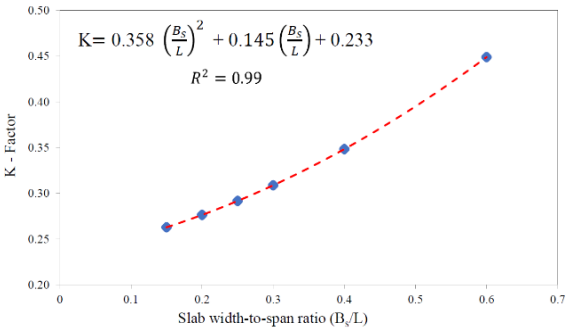

Fig. 19 The factor "K" against the slab width-to-span ratio (B_s/L)

Table 2 C, K, M and K_{mod}. factors.

Slab thickness	B_s/L	C	K	M= C/B_s/L	K_{mod}	B_{es} EQ / B_{es} FE	% S.D
	0.15	22.39	0.26	3.36	0.26	1.04	0.93
	0.20	16.59	0.28	3.32	0.28	1.04	2.33
250	0.25	13.33	0.29	3.33	0.29	1.04	3.07
	0.30	11.24	0.31	3.37	0.31	1.03	2.60
	0.40	8.48	0.35	3.39	0.35	1.03	3.83
	0.60	5.68	0.45	3.41	0.45	0.83	4.56
AVG				3.36			
	0.15	21.65	0.26	3.25	0.26	1.04	1.06
	0.20	16.06	0.28	3.21	0.28	1.05	2.26
300	0.25	12.79	0.29	3.20	0.29	1.05	2.28
	0.30	10.82	0.31	3.25	0.31	1.04	3.37
	0.40	8.08	0.35	3.23	0.35	1.04	4.19
	0.60	5.42	0.45	3.25	0.45	0.84	6.21
AVG				3.23			
	0.15	20.79	0.26	3.12	0.26	1.02	0.97
	0.20	15.26	0.28	3.05	0.28	1.04	1.38
350	0.25	12.17	0.29	3.04	0.29	1.05	2.25
	0.30	10.24	0.31	3.07	0.31	1.04	3.16
	0.40	7.60	0.35	3.04	0.35	1.05	3.79
	0.60	5.10	0.45	3.06	0.45	0.85	6.47
AVG				3.06			
	0.15	19.78	0.26	2.97	0.26	1.01	1.18
	0.20	14.56	0.28	2.91	0.28	1.03	1.48
400	0.25	11.55	0.29	2.89	0.29	1.04	2.18
	0.30	9.67	0.31	2.90	0.31	1.03	2.89
	0.40	7.42	0.35	2.97	0.35	1.01	4.24
	0.60	4.97	0.45	2.98	0.45	0.91	4.72
AVG				2.94			

Table 3 M factor with different t_s.

t_s	t_s/B_s	M
250	0.04	3.36
300	0.05	3.23
350	0.06	3.06
400	0.07	2.94
250	0.04	3.36
300	0.05	3.23

6.2 validation of the proposed equation for (Bes) with experimental programs

The proposed equation was validated using three independent experimental programs reported in Refs. [12, 13, 18]. The effective slab-width-to-span ratios obtained from these studies were compared with the predictions of the proposed numerical equation at the service limit state. As shown in Fig. 20, the experimental results exhibit very close agreement with the proposed model.

The average ratio between the effective slab widths calculated using the proposed Eq. (5) and those obtained from the experimental programs is 1.00, with a standard deviation of 7 percent, as presented in Table 4. This strong correspondence confirms the accuracy and reliability of the proposed equation and demonstrates its suitability for predicting the effective slab width of BGCSs at the service limit state.

6.3 Comparison between Lasheen's numerical approach and the equation of the current study

A comparison between the equation proposed by (Lasheen et al., 2018) and Eq. (9) developed in the present study shows a clear difference in predictive accuracy. When evaluated against the independent experimental programs and the second phase of the current parametric study, the average ratio between the effective slab widths predicted by Lasheen et al.'s equation and the corresponding reference values is 0.93, with a standard deviation of 8.5 percent. In contrast, the proposed Eq. (9) in this study yields an average ratio of 1.00, with a standard deviation of 6.9 percent. These results demonstrate that the equation developed in the present study provides more accurate and reliable predictions of the effective slab width.

The improved accuracy of the proposed equation is primarily attributed to the broader scope of parametric investigation, which considered a wider range of spans. This expanded range introduced slab thickness as an additional influential parameter in determining the effective slab width. Consequently, the sensitivity of the proposed equation is enhanced, leading to more precise predictions compared with the equation developed by (Lasheen et al., 2018).

For slab-thickness-to-slab-width ratios greater than 0.05, as encountered in the specimens studied by (Lasheen et al., 2018), Eqs. (5) through (9) exhibit strong agreement. However, when this ratio falls below 0.05, the discrepancy between the two equations becomes significant, with deviations averaging approximately 20 percent, as reported in Tables 4 and 5. These findings underscore the importance of considering both span length and slab thickness in the structural design of composite girders.

When the slab thickness is relatively large compared with the span length, the effective slab width is predominantly governed by the span. Conversely, as the slab becomes thinner, its influence on the effective slab width becomes more pronounced. Thus, accurate determination of the effective slab width requires accounting for both parameters to ensure reliable and precise structural design. These observations confirm the enhanced sensitivity and accuracy of the equation developed in the present study relative to that of (Lasheen et al., 2018).

Table 4 Comparison between Eq (5) & Eq (5) with respect to experimental programs.

Eq. (no.) / Exp. Program	AVG	SD
Eq (5)	0.93	0.085
Eq (9)	1.00	0.069

Table 5 Comparison between Eq (5) & Eq (5) with respect to current study girders.

Eq. (no.) / Exp. Program	AVG	SD
Eq (5)	0.80	0.073
Eq (9)	1.00	0.028

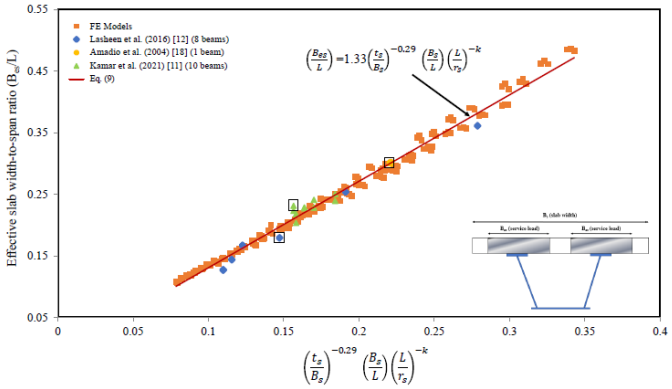

Fig. 20 FEA versus researches for effective slab width at service limits states (B_{es}).

Codes comparison for the proposed equation for (B_{es})

Figure 21 illustrates the relationship between the parameter (t_s/B_s)-0.29(B_s/L) (L/r_s)$^{-k}$ on the horizontal axis and the effective-slab-width-to-span ratio (Bes/L) on the vertical axis. The provisions of (AASHTO, 2017) and (Eurocode 4, 2005) are plotted on the same graph for comparison. The results show that the (AASHTO, 2017) provisions consistently underestimate the effective slab width by approximately 25% when compared with the values predicted by the proposed Eq. (9). In contrast, the EN 1994-2-2 provisions tend to overestimate the effective width by about 20% relative to Eq. (9).

The underestimation in AASHTO (2017) and overestimation in EN 1994-2-2 can be attributed to the differences in their underlying methodologies. AASHTO (2017) incorporates the concrete slab thickness when determining the effective slab width, which results in more conservative values. EN 1994-2-2 does not account for slab thickness, which leads to larger effective width predictions. Both provisions limit the effective-slab-width-to-span ratio (B_{es}/L) to a maximum of 0.25 at the

service limit state. This upper limit can significantly underestimate the effective slab width for girders with wide concrete slabs, where the steel section can engage a larger portion of the slab in resisting compressive stresses.

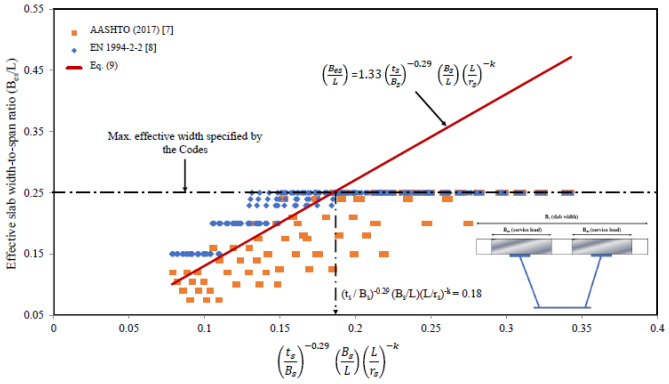

Fig. 21 Comparison between the proposed equation for (B_{es}) and that given by the AASHTO (2017) & EN 1994-2-2.

7. Conclusions

This study proposes a new design formulation for determining the effective slab width of steel–concrete composite box girder sections (BGCSs) at the service limit state. The formulation was developed through an extensive nonlinear finite element parametric study and validated against three independent experimental programs, conducted by (Lasheen et al., 2016), (Kamar et al., 2021), and (Macorini et al., 2006). The results indicate that the proposed equation provides accurate and consistent predictions of effective slab width over a wide range of geometric configurations and offers improved agreement compared with existing code-based provisions.

The effective slab width in BGCSs is governed by the interaction of three key parameters: the girder slenderness ratio (L/rs), the slab-width-to-span ratio (Bs/L), and the slab-thickness-to-slab-width ratio (ts/Bs). Unlike existing formulations, the proposed approach explicitly accounts for slab thickness, which becomes increasingly influential for long-span girders. Relative to AASHTO (2017) and Eurocode 4 (2005), the proposed model reduces systematic bias, as AASHTO underestimates the effective slab width by up to 25%, whereas Eurocode 4 overestimates it for wide decks by up to 20%.

The study also shows that shear lag in the steel bottom flange has a negligible influence on the effective concrete slab width, supporting common assumptions in current practice. Overall, the proposed formulation extends the applicability of existing approaches to modern BGCSs with wide decks and long spans under static four-point bending.

This work is limited to simply supported BGCSs subjected to static loading. Dynamic effects, moving loads, and time-dependent phenomena (creep, shrinkage, and temperature) were not considered. Although the formulation was validated against available experimental data, additional large-scale tests for long-span BGCSs with varying slab thicknesses are recommended.

Future research should extend the methodology to continuous and multi-span systems, quantify the influence of dynamic and fatigue loading, and incorporate time-dependent effects to further improve prediction accuracy and support the development of comprehensive design provisions for composite box girder bridges.

References

ABAQUS (2014). *Theory Manual Version 6.14*. Dassault Systèmes, France.

Lasheen, M., Shaat, A. & Khalil, A. (2018). Numerical evaluation for the effective slab width of steel–concrete composite girders. *Journal of Constructional Steel Research*, 148, 124–137. https://doi.org/10.1016/j.jcsr.2018.05.015.

Chen, J., Wang, W. & Ding, F.X. (2019). Behavior of an advanced bolted shear connector in prefabricated steel–concrete composite girders. *Materials*, 12(18), 2958. https://doi.org/10.3390/ma12182958.

Zhu, L., Nie, J.G. & Li, F.X. (2015). Simplified analysis method accounting for shear-lag effect of steel–concrete composite decks. *Journal of Constructional Steel Research*, 115, 62–80. https://doi.org/10.1016/j.jcsr.2015.08.020.

Nicoletti, R., Alexandre, R., Alex, S. & Carlos, M. (2021). Numerical assessment of effective width in steel–concrete composite box girder bridges. *Advanced Structural Engineering*, 24(5), 977–994. https://doi.org/10.1177/1369433220971744.

Sedlacek, G. & Bild, S. (1993). A simplified method for the determination of the effective width due to shear lag effects. *Journal of Constructional Steel Research*, 24, 155–182. https://doi.org/10.1016/0143-974X(93)90042-Q.

Gara, F., Leoni, G., Tarantino, A. & Dezi, L. (2001). Time-dependent analysis of shear-lag effect in composite girders. *Journal of Engineering Mechanics*, 127(1), 71–79. https://doi.org/10.1061/(ASCE)0733-9399(2001)127:1(71).

Adekola, A. O. (1968). Effective widths of composite beams of steel and concrete. The Structural Engineer, 46(9), 285–289.

Adekola, A. O. (1974). The dependence of shear-lag on partial interaction in composite beams. International Journal of Solids and Structures, 10, 389–400. https://doi.org/10.1016/0020-7683(74)90108-5

Gara, F., Ranzi, G., & Leoni, G. (2008). Analysis of the shear lag effect in composite bridges with complex static schemes by means of a deck finite element. International Journal of Steel Structures, 8(4), 249–260.

Giaccu, G. F., Briseghella, B., & Fenu, L. (2022). Numerical simulation and simplified calculation of the effective slab width for composite cable-stayed bridges. Structures, 39, 512–526. https://doi.org/10.1016/j.istruc.2022.03.034

Giaccu, G. F., Maiorana, E., Fenu, L., & Briseghella, B. (2025). Calculating shear lag in steel-concrete composite beams under combined compression and bending. Engineering Structures, 322, 119101. https://doi.org/10.1016/j.engstruct.2024.119101

Huitong, X., Jinzhu, G., Qi, M., Li, X., & Xu, Z. (2019). Simplified analysis method considering shear-lag effect of steel–concrete composite decks. In IOP Conference Series: Earth and Environmental Science (EES). https://doi.org/10.1088/1755-1315/371/2/022003

AASHTO (2017). *LRFD Bridge Design Specifications*. American Association of State Highway and Transportation Officials, Washington, DC.

Eurocode 4 (2005). *Design of Composite Steel and Concrete Structures — Part 2: General Rules and Rules for Bridges (EN 1994-2)*. European Committee for Standardization, Brussels.

Alemayehu, D. (2013). *Study of Shear Lag Effect in Box Girder Bridges*. MSc Thesis, Indian Institute of Technology, Delhi.

Yao, T.H. & Chung, C.F. (2002). Application of EBEF method for the distortional analysis of steel box girder bridge superstructures during construction. *Advanced Structural Engineering*, 5(4), 279–288. https://doi.org/10.1260/136943302320974581.

Kamar, A., Lasheen, M., Shaat, A., Zaher, A. & Khalil, A. (2021). Factors affecting slip and stress distribution of concrete slabs in composite girders. *Engineering Structures*, 245, 112880. https://doi.org/10.1016/j.engstruct.2021.112880.

Lasheen, M., Shaat, A. & Khalil, A. (2016). Behaviour of lightweight concrete slab acting compositely with steel I-sections. *Construction and Building Materials*, 124, 967–981. https://doi.org/10.1016/j.conbuildmat.2016.08.007.

Baskar, K., Shanmugam, N.E. & Thevendran (2002). Finite element analysis of steel–concrete composite plate girder. *Journal of Structural Engineering (ASCE)*, 128(9), 1158–1168. https://doi.org/10.1061/(ASCE)0733-9445(2002)128:9(1158).

Liang, Q.Q., Uy, B., Bradford, M.A. & Ronagh, H.R. (2004). Ultimate strength of continuous composite girders in combined bending and shear. *Journal of Constructional Steel Research*, 60(8), 1109–1128. https://doi.org/10.1016/j.jcsr.2003.12.001.

Liang, Q.Q., Uy, B., Bradford, M.A. & Ronagh, H.R. (2005). Strength analysis of steel–concrete composite girders in combined bending and shear. *Journal of Structural Engineering (ASCE)*, 131(10), 1593–1603. https://doi.org/10.1061/(ASCE)0733-9445(2005)131:10(1593).

Ryu, H.K., Shim, C.S. & Chang, S.P. (2004). Testing a composite box-girder bridge with precast decks. *Proceedings of the Institution of Civil Engineers – Structures and Buildings*, 157(4), 243–250. https://doi.org/10.1680/stbu.2004.157.4.243.

Macorini, L., Fragiacomo, M., Amadio, C. & Izzuddin, B.A. (2006). Long-term analysis of steel–concrete composite beams: FE modelling for effective width evaluation. *Engineering Structures*, 28(8), 1110–1121. https://doi.org/10.1016/j.engstruct.2005.12.002.

Disclaimer

Annexture

Table 1A Ultimate loads (Pu) for all girders

ID	Pu Calc. (KN) × 10^3	Pu FE (KN) × 10^3	$\frac{P_u\ Calc.}{P_u\ FE}$	ID	Pu Calc. (KN) × 10^3	Pu FE (KN) × 10^3	$\frac{P_u\ Calc.}{P_u\ FE}$
B1	16.99	16.99	1	B34	10.269	10.269	1
B2	13.053	13.457	0.97	B35	8.188	8.188	1
B3	10.33	10.874	0.95	B36	6.033	6.033	1
B4	8.689	8.689	1	B37	20.324	20.324	1
B5	6.827	6.966	0.98	B38	14.804	15.421	0.96
B6	5.03	5.186	0.97	B39	11.302	12.42	0.91
B7	16.903	16.903	1	B40	9.552	9.552	1
B8	13.506	13.642	0.99	B41	7.505	7.658	0.98
B9	11.022	11.134	0.99	B42	5.53	5.701	0.97
B10	9.273	9.273	1	B43	20.709	20.709	1
B11	7.286	7.286	1	B44	15.692	15.851	0.99
B12	5.368	5.368	1	B45	12.099	12.221	0.99
B13	16.508	16.675	0.99	B46	10.162	10.162	1
B14	13.768	14.342	0.96	B47	8.045	8.045	1
B15	11.577	12.187	0.95	B48	5.928	5.988	0.99
B16	9.784	9.883	0.99	B49	20.786	21.21	0.98
B17	7.687	7.765	0.99	B50	16.39	17.253	0.95
B18	5.664	5.664	1	B51	12.885	13.708	0.94
B19	18.711	18.711	1	B52	10.734	10.842	0.99
B20	14.021	14.021	1	B53	8.571	8.746	0.98
B21	10.797	10.797	1	B54	6.315	6.379	0.99
B22	9.111	9.111	1	B55	21.829	22.049	0.99
B23	7.158	7.158	1	B56	15.447	15.447	1
B24	5.275	5.275	1	B57	11.845	11.965	0.99
B25	18.861	19.051	0.99	B58	9.992	9.992	1
B26	14.691	15.303	0.96	B59	7.851	7.851	1
B27	11.578	12.449	0.93	B60	5.785	5.785	1
B28	9.701	9.799	0.99	B61	22.449	22.908	0.98
B29	7.677	7.914	0.97	B62	16.51	17.564	0.94
B30	5.657	5.831	0.97	B63	12.66	14.225	0.89
B31	18.701	18.89	0.99	B64	10.64	10.747	0.99
B32	15.171	15.481	0.98	B65	8.418	8.678	0.97
B33	12.329	12.329	1	B66	6.203	6.461	0.96
B67	22.762	22.992	0.99	B114	8.294	8.55	0.97
B68	17.426	17.781	0.98	B115	31.304	31.304	1
B69	13.462	13.598	0.99	B116	23.392	23.628	0.99
B70	11.232	11.345	0.99	B117	18.072	18.441	0.98
B71	8.971	8.971	1	B118	15.069	15.069	1
B72	6.61	6.677	0.99	B119	11.908	11.908	1
B73	26.309	26.309	1	B120	8.774	8.863	0.99
B74	19.904	19.904	1	B121	31.673	32.319	0.98
B75	15.924	16.248	0.98	B122	24.203	25.748	0.94
B76	13.407	13.407	1	B123	19.056	20.272	0.94
B77	10.534	10.86	0.97	B124	15.794	15.953	0.99
B78	7.762	7.762	1	B125	12.556	12.683	0.99
B79	26.467	26.467	1	B126	9.252	9.345	0.99
B80	20.453	20.453	1	B127	32.73	32.73	1
B81	16.661	16.496	1.01	B128	23.368	23.604	0.99
B82	14.12	14.12	1	B129	17.648	17.826	0.99
B83	11.094	10.771	1.03	B130	14.811	14.811	1
B84	8.175	8.175	1	B131	11.637	11.637	1
B85	26.432	26.432	1	B132	8.575	8.575	1
B86	20.869	20.869	1	B133	33.518	34.202	0.98
B87	17.294	17.294	1	B134	24.53	26.663	0.92
B88	14.624	14.624	1	B135	18.651	20.724	0.9
B89	11.49	11.49	1	B136	15.58	15.898	0.98
B90	8.466	8.382	1.01	B137	12.312	12.825	0.96
B91	28.588	28.588	1	B138	9.072	9.45	0.96
B92	21.283	21.283	1	B139	34.094	34.438	0.99
B93	16.556	16.556	1	B140	25.544	25.802	0.99
B94	13.85	13.85	1	B141	19.649	19.847	0.99
B95	10.882	10.882	1	B142	16.307	16.471	0.99
B96	8.018	8.018	1	B143	12.977	13.108	0.99
B97	28.953	28.953	1	B144	9.562	9.659	0.99
B98	22.033	22.951	0.96	B145	15.46	15.617	1
B99	17.494	18.415	0.95	B146	11.392	11.507	1
B100	14.59	14.59	1	B147	38.744	38.744	1
B101	11.523	11.64	0.99	B148	28.148	28.148	1

B102	8.491	8.577	0.99	B149	21.926	22.147	1
B103	29.119	29.119	1	B150	18.288	18.288	1
B104	22.644	22.644	1	B151	14.369	14.369	1
B105	18.324	18.51	0.99	B152	10.588	10.588	1
B106	15.307	15.307	1	B153	39.691	40.918	1
B107	12.161	12.161	1	B154	29.418	30.967	1
B108	8.961	8.961	1	B155	23.34	23.34	1
B109	30.728	30.728	1	B156	19.531	19.93	1
B110	22.438	23.87	0.94	B157	15.409	15.886	1
B111	17.082	18.368	0.93	B158	11.354	11.354	0.96
B112	14.326	14.326	1	B159	40.271	40.678	0.95
B113	11.256	11.485	0.98	B160	30.463	30.77	1
B161	24.59	24.59	0.99	B189	44.904	44.904	0.97
B162	20.62	20.62	0.99	B190	32.455	32.783	0.96
B163	16.44	16.44	1	B191	24.702	23.982	0.97
B164	12.113	12.236	1	B192	20.551	20.348	1
B165	41.142	42.856	0.99	B193	16.228	17.082	0.99
B166	29.523	31.077	1	B194	11.957	12.456	0.99
B167	22.499	22.727	1	B195	46.045	43.853	1
B168	18.777	18.967	1	B196	34.017	30.925	0.96
B169	14.754	15.695	0.97	B197	26.315	27.592	1
B170	10.871	10.763	0.95	B198	21.776	22.69	0.99
B171	42.369	26.933	1	B199	17.286	18.79	0.98
B172	31.052	27.82	0.98	B200	12.737	13.696	0.94
B173	24.106	24.927	0.97	B201	23078	24551	0.94
B174	20.024	20.891	1	B202	19290	19485	0.99
B175	15.806	16.294	0.99	B203	15156	15309	0.99
B176	11.646	11.646	0.99	B204	11168	11281	0.99
B177	43.229	43.666	1	B205	44904	44904	1
B178	32.356	32.682	1	B206	32455	32783	0.99
B179	25.606	25.606	1	B207	24702	23982	1.03
B180	21.247	22.165	0.99	B208	20551	20348	1.01
B181	16.851	16.851	0.96	B209	16228	17082	0.95
B182	12.416	12.542	0.95	B210	11957	12456	0.96
B183	43.397	44.283	0.99	B211	46045	43853	1.05
B184	30.668	32.625	0.99	B212	34017	30925	1.1
B185	23.078	24.551	0.94	B213	26315	27592	0.95
B186	19.29	19.485	1.01	B214	21776	22690	0.96
B187	15.156	15.309	1.57	B215	17286	18790	0.92
B188	11.168	11.281	1.12	B216	12737	13696	0.93

Table 2A Effective slab width at service limit state for all girders

ID	F.E B_{es} (mm)	Proposed B_{es} (mm)	Proposed B_{es} / B_{es} FE	ID	F.E B_{es} (mm)	Proposed B_{es} (mm)	Proposed B_{es} / B_{es} FE
B1	3216	3333	1.04	B16	4729	4796	1.01
B2	4163	4338	1.04	B17	4834	4864	1.01
B3	4581	4729	1.03	B18	4895	4836	0.99
B4	4686	4861	1.04	B19	3042	3160	1.04
B5	4789	4926	1.03	B20	3937	4112	1.04
B6	4889	4895	1.00	B21	4346	4483	1.03
B7	3238	3298	1.02	B22	4457	4608	1.03
B8	4200	4303	1.02	B23	4567	4669	1.02
B9	4614	4695	1.02	B24	4677	4640	0.99
B10	4717	4828	1.02	B25	3066	3126	1.02
B11	4819	4894	1.02	B26	3977	4079	1.03
B12	4877	4865	1.00	B27	4381	4451	1.02
B13	3233	3265	1.01	B28	4492	4576	1.02
B14	4203	4269	1.02	B29	4603	4639	1.01
B15	4622	4662	1.01	B30	4713	4611	0.98
B31	3063	3095	1.01	B78	5363	5464	1.02
B32	3983	4046	1.02	B79	3957	3994	1.01
B33	4394	4420	1.01	B80	4918	4991	1.01
B34	4508	4546	1.01	B81	5328	5356	1.01
B35	4623	4610	1.00	B82	5351	5467	1.02
B36	4738	4584	0.97	B83	5370	5506	1.03
B37	2866	3020	1.05	B84	5389	5441	1.01
B38	3710	3930	1.06	B85	3940	3965	1.01
B39	4120	4285	1.04	B86	4905	4964	1.01
B40	4237	4404	1.04	B87	5324	5329	1.00
B41	4353	4463	1.03	B88	5352	5442	1.02
B42	4472	4434	0.99	B89	5376	5482	1.02
B43	2891	2988	1.03	B90	5397	5419	1.00
B44	3751	3898	1.04	B91	3781	3813	1.01
B45	4146	4254	1.03	B92	4691	4758	1.01
B46	4265	4374	1.03	B93	5067	5102	1.01
B47	4385	4434	1.01	B94	5110	5206	1.02
B48	4470	4407	0.99	B95	5148	5242	1.02
B49	2893	2958	1.02	B96	5185	5180	1.00
B50	3761	3867	1.03	B97	3795	3786	1.00
B51	4164	4224	1.01	B98	4717	4731	1.00
B52	4287	4345	1.01	B99	5100	5076	1.00
B53	4411	4406	1.00	B100	5139	5182	1.01
B54	4536	4381	0.97	B101	5177	5219	1.01
B55	2769	2904	1.05	B102	5212	5158	0.99
B56	3584	3779	1.05	B103	3772	3759	1.00
B57	3885	4120	1.06	B104	4695	4705	1.00
B58	4009	4235	1.06	B105	5093	5052	0.99
B59	4134	4291	1.04	B106	5139	5158	1.00
B60	4261	4264	1.00	B107	5182	5196	1.00
B61	2794	2873	1.03	B108	5221	5136	0.98
B62	3625	3748	1.03	B109	3568	3644	1.02
B63	3925	4090	1.04	B110	4427	4547	1.03
B64	4050	4206	1.04	B111	4810	4876	1.01
B65	4177	4264	1.02	B112	4872	4976	1.02
B66	4307	4238	0.98	B113	4931	5010	1.02
B67	2803	2844	1.01	B114	4988	4950	0.99
B68	3644	3719	1.02	B115	3580	3618	1.01
B69	3946	4062	1.03	B116	4450	4522	1.02
B70	4076	4178	1.03	B117	4838	4852	1.00
B71	4208	4237	1.01	B118	4899	4953	1.01
B72	4342	4213	0.97	B119	4958	4988	1.01
B73	3956	4023	1.02	B120	5015	4930	0.98
B74	4909	5019	1.02	B121	3577	3593	1.00
B75	5290	5382	1.02	B122	4452	4497	1.01
B76	5318	5493	1.03	B123	4832	4828	1.00
B77	5342	5531	1.04	B124	4900	4930	1.01
B125	4965	4966	1.00	B171	42.369	26.933	1
B126	5027	4909	0.98	B172	31.052	27.82	0.98
B127	3491	3504	1.00	B173	24.106	24.927	0.97
B128	4331	4373	1.01	B174	20.024	20.891	1
B129	4551	4689	1.03	B175	15.806	16.294	0.99
B130	4632	4785	1.03	B176	11.646	11.646	0.99
B131	4709	4818	1.02	B177	43.229	43.666	1
B132	4738	4760	1.00	B178	32.356	32.682	1
B133	3515	3479	0.99	B179	25.606	25.606	1

B134	4368	4348	1.00	B180	21.247	22.165	0.99
B135	4576	4665	1.02	B181	16.851	16.851	0.96
B136	4657	4762	1.02	B182	12.416	12.542	0.95
B137	4736	4797	1.01	B183	43.397	44.283	0.99
B138	4763	4740	1.00	B184	30.668	32.625	0.99
B139	3476	3454	0.99	B185	23.078	24.551	0.94
B140	4326	4324	1.00	B186	19.29	19.485	1.01
B141	4573	4643	1.02	B187	15.156	15.309	1.57
B142	4661	4740	1.02	B188	11.168	11.281	1.12
B143	4746	4776	1.01	B189	44.904	44.904	0.97
B144	4778	4720	0.99	B190	32.455	32.783	0.96
B145	4613	4613	0.95	B191	24.702	23.982	0.97
B146	5582	5582	0.96	B192	20.551	20.348	1
B147	5914	5914	0.99	B193	16.228	17.082	0.99
B148	6000	6000	1.00	B194	11.957	12.456	0.99
B149	6000	6000	1.02	B195	46.045	43.853	1
B150	5920	5920	1.02	B196	34.017	30.925	0.96
B151	4579	4579	0.94	B197	26.315	27.592	1
B152	5550	5550	0.95	B198	21.776	22.69	0.99
B153	5884	5884	0.98	B199	17.286	18.79	0.98
B154	5975	5975	1.00	B200	12.737	13.696	0.94
B155	5990	5990	1.01	B201	23078	24551	0.94
B156	5895	5895	1.01	B202	19290	19485	0.99
B157	4546	4546	0.94	B203	15156	15309	0.99
B158	5519	5519	0.94	B204	11168	11281	0.99
B159	40.271	40.678	0.95	B205	44904	44904	1
B160	30.463	30.77	1	B206	32455	32783	0.99
B161	24.59	24.59	0.99	B207	24702	23982	1.03
B162	20.62	20.62	0.99	B208	20551	20348	1.01
B163	16.44	16.44	1	B209	16228	17082	0.95
B164	12.113	12.236	1	B210	11957	12456	0.96
B165	41.142	42.856	0.99	B211	46045	43853	1.05
B166	29.523	31.077	1	B212	34017	30925	1.1
B167	22.499	22.727	1	B213	26315	27592	0.95
B168	18.777	18.967	1	B214	21776	22690	0.96
B169	14.754	15.695	0.97	B215	17286	18790	0.92
B170	10.871	10.763	0.95	B216	12737	13696	0.93